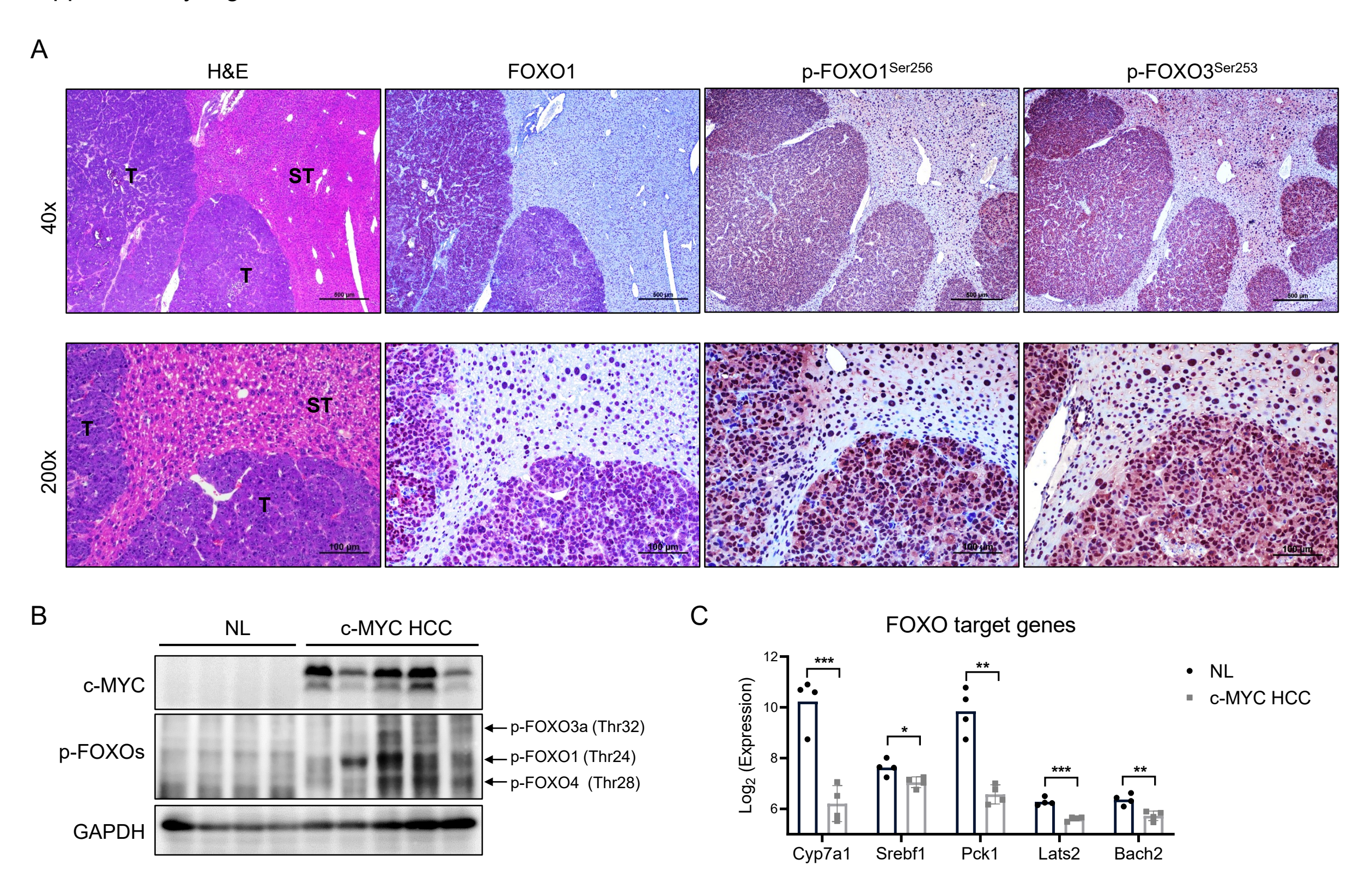
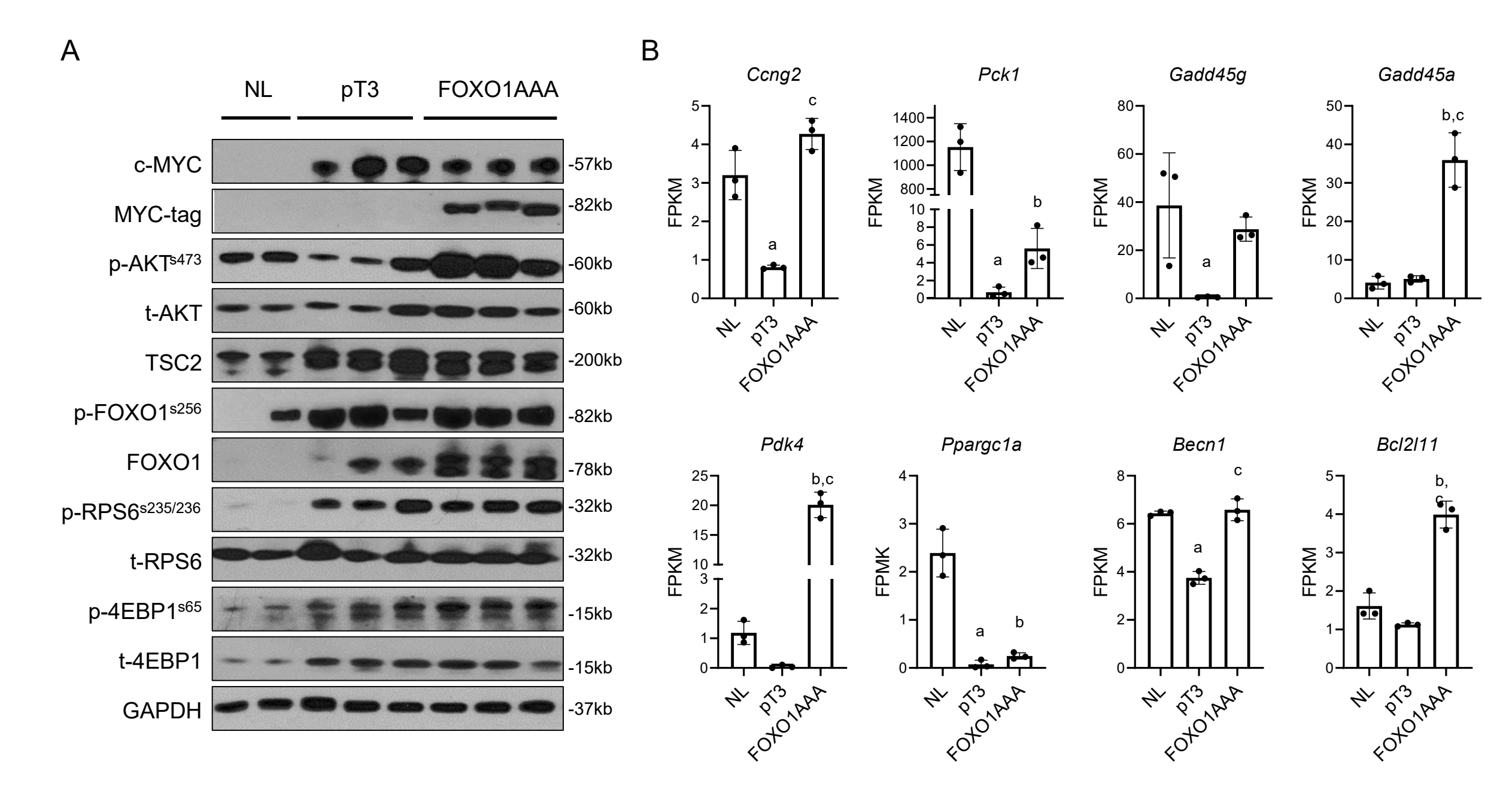
TSC/mTORC1 mediates mTORC2/AKT1 signaling in c-MYC-induced murine hepatocarcinogenesis via centromere protein M

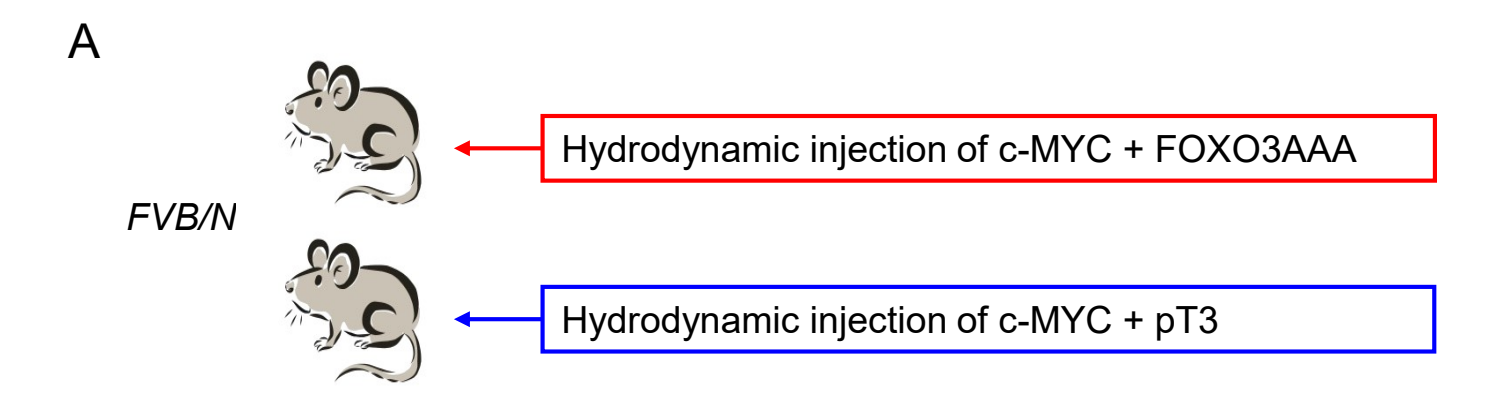
Yi Zhou^{1, 2*}, Shu Zhang^{3,4*}, Guoteng Qiu^{5,6}, Xue Wang⁷, Andrew Yonemura⁷,
Hongwei Xu^{2,5}, Guofei Cui^{2,7}, Shanshan Deng^{2,7}, Joanne Chun⁷, Nianyong Chen^{3,4,8},
Meng Xu⁹, Xinhua Song¹⁰, Jingwen Wang¹⁰, Zijing Xu¹⁰, Youping Deng^{7,11}, Matthias
Evert¹², Diego F. Calvisi¹², Shumei Lin¹, Haichuan Wang^{5,6} and Xin Chen^{2,7}

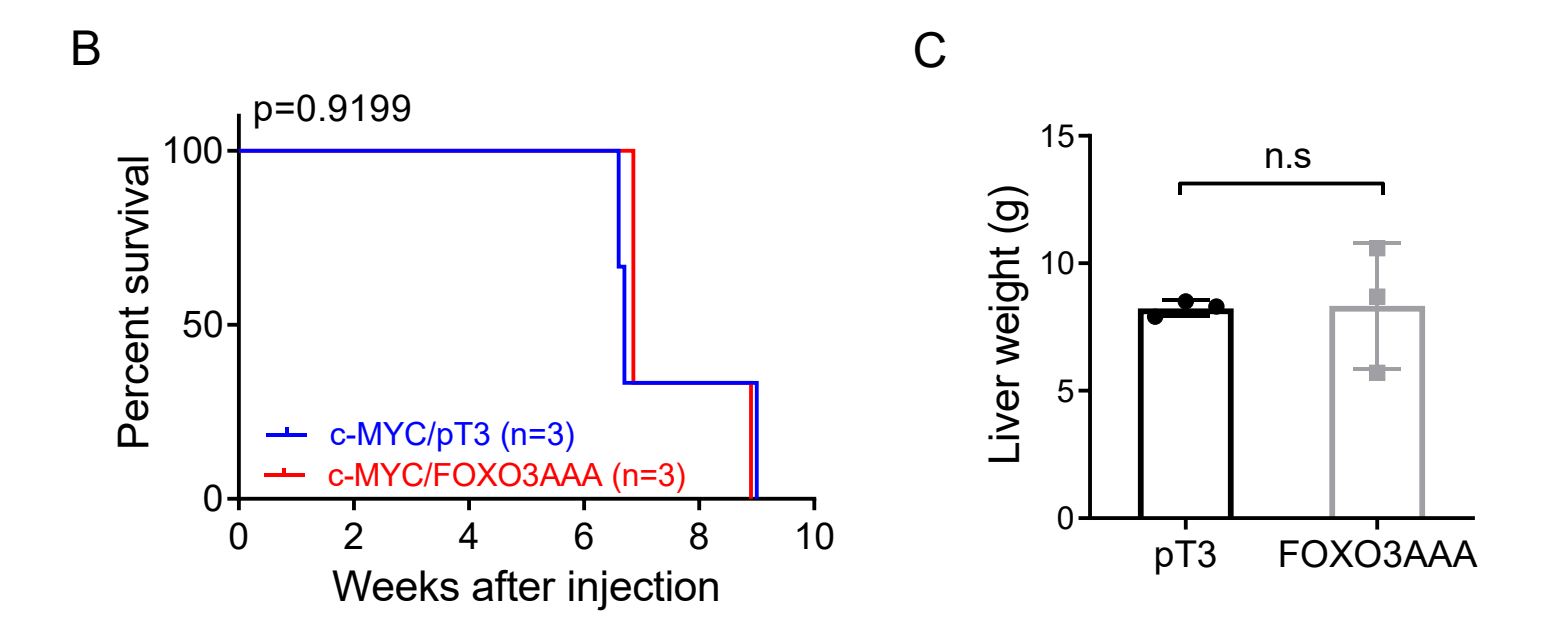


Supplementary Fig. 1. Activation status of FOXO1 in murine c-MYC HCC. (A) Representative images: H&E staining, and immunohistochemical staining of FOXO1, p-FOXO1^{Ser256}, and p-FOXO3^{Ser253}. Scale bars: 500 μ m for 40 \times images and 100 μ m for 200 \times images. (B) Western blot results show the expression of c-MYC and p-FOXOs in normal livers (NL) and c-Myc HCCs. GAPDH was used as the loading control. (C) Microarray analysis of FOXO1 downstream genes in normal livers (NL) and c-Myc HCCs (n = 4, 4). Student's t-test. *, p<0.05. **, p<0.01. ***, p<0.001.

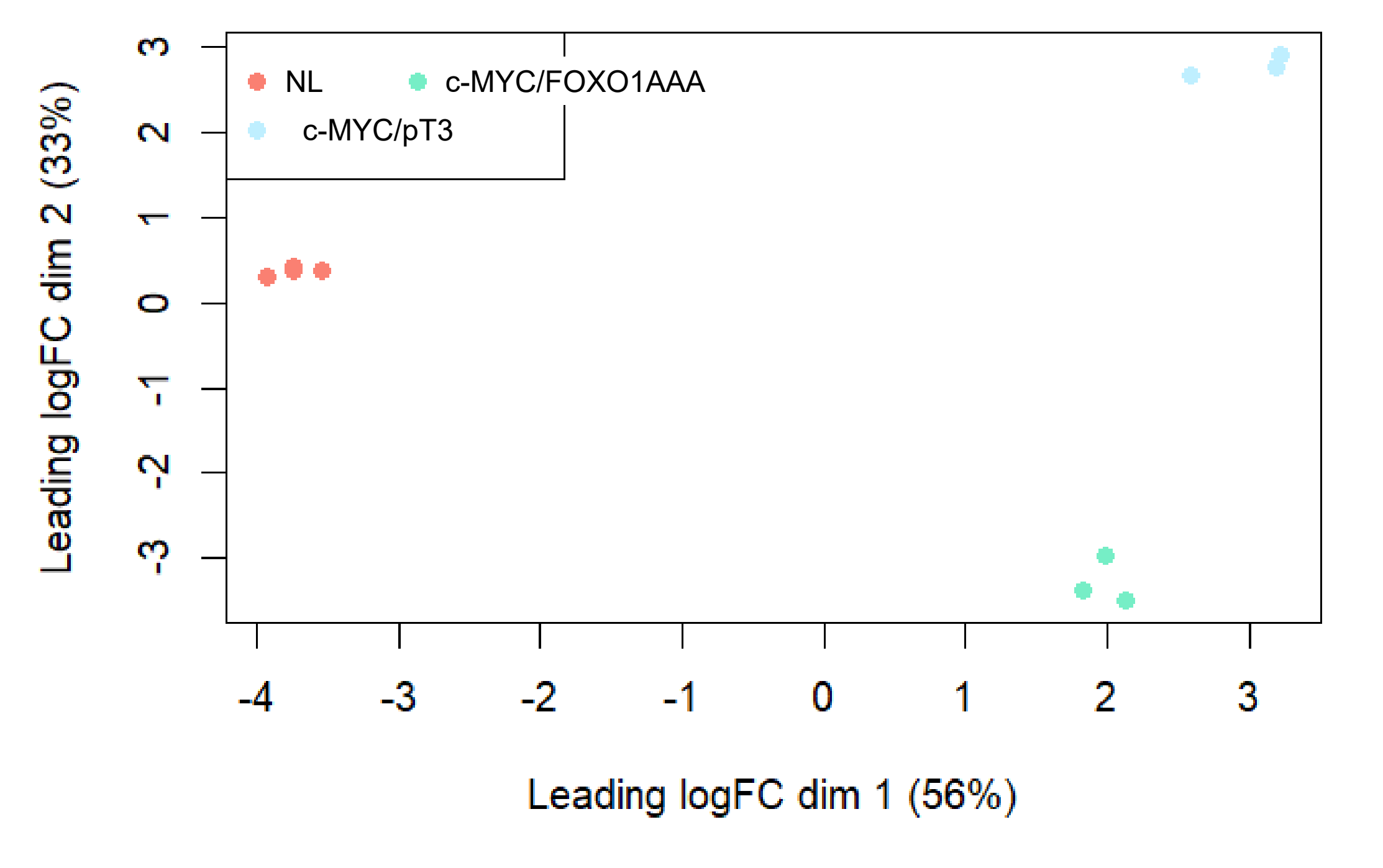


Supplementary Fig. 2. Effects of FOXO1 activation on c-MYC liver tumors. (A) Western blot results show the levels of c-MYC, MYC-tagged FOXO1AAA, and key molecules downstream of mTORC2 signaling. GAPDH was used as the loading control. (B) RNAseq results of FOXO1 target genes in the c-MYC/pT3 and c-MYC/FOXO1AAA HCCs (n = 3, 3). Data are presented as mean \pm SD. Tukey–Kramer test. At least p<0.05. a, versus NL; b, versus pT3; c, versus NL. Abbreviations: NL, normal liver. pT3, pT3-EF1 α .

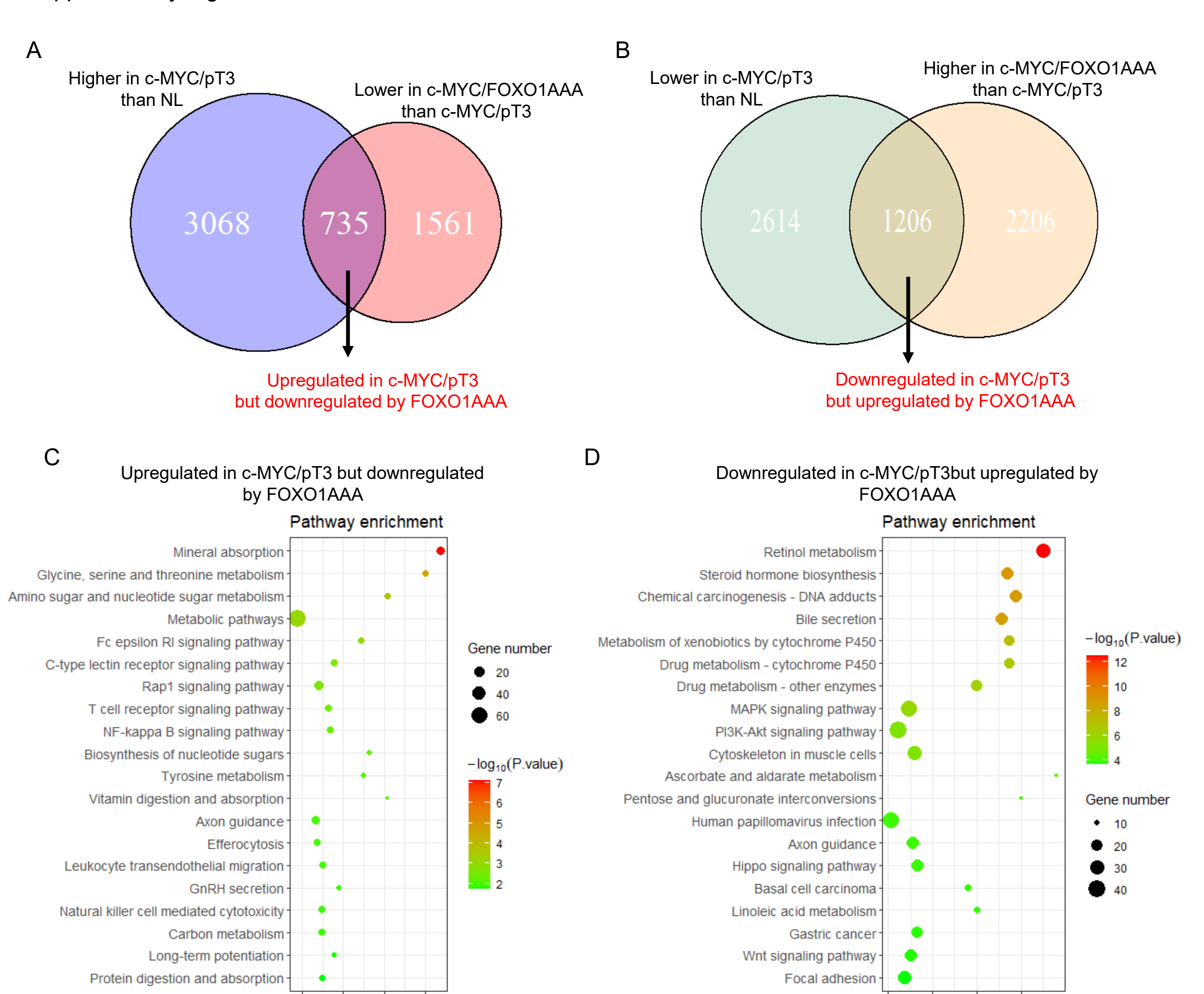




Supplementary Fig. 3. Effect of FOXO3 activation on c-MYC-induced hepatocarcinogenesis. (A) Study design. FVB/N mice were hydrodynamically injected with plasmid mixtures of c-MYC and a constitutively active mutant form of FOXO3 (FOXO3AAA) in pT3-EF1 α backbone (c-MYC/FOXO3AAA, n = 3). The control mice were hydrodynamically injected with c-MYC and pT3-EF1 α empty vector (c-MYC/pT3, n = 3). Mice were monitored for tumor development and were euthanized when moribund tumors developed or till the end of the observation period. (B) Survival curve of mice in two groups. The Kaplan-Meier comparison was performed, p = 0.9199. (C) Comparison of liver weight between the two groups. Data are presented as mean \pm SD. Student's t-test. ns, no significant. Abbreviations: pT3, pT3-EF1 α .



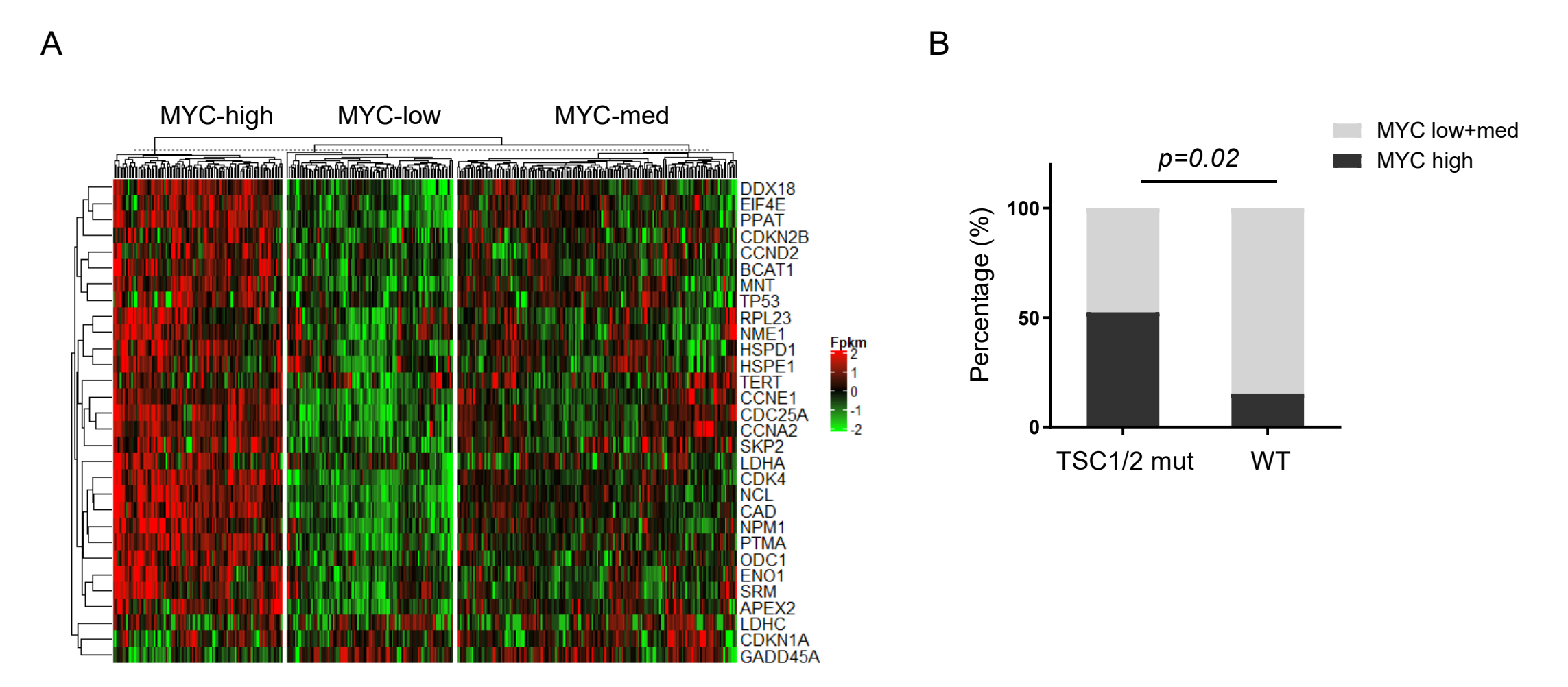
Supplementary Fig. 4. Principal component analysis (PCA) of RNA-seq data for normal liver (NL), c-MYC/pT3, and c-MYC/FoxO1AAA in mouse model (n = 3, 3, 3).



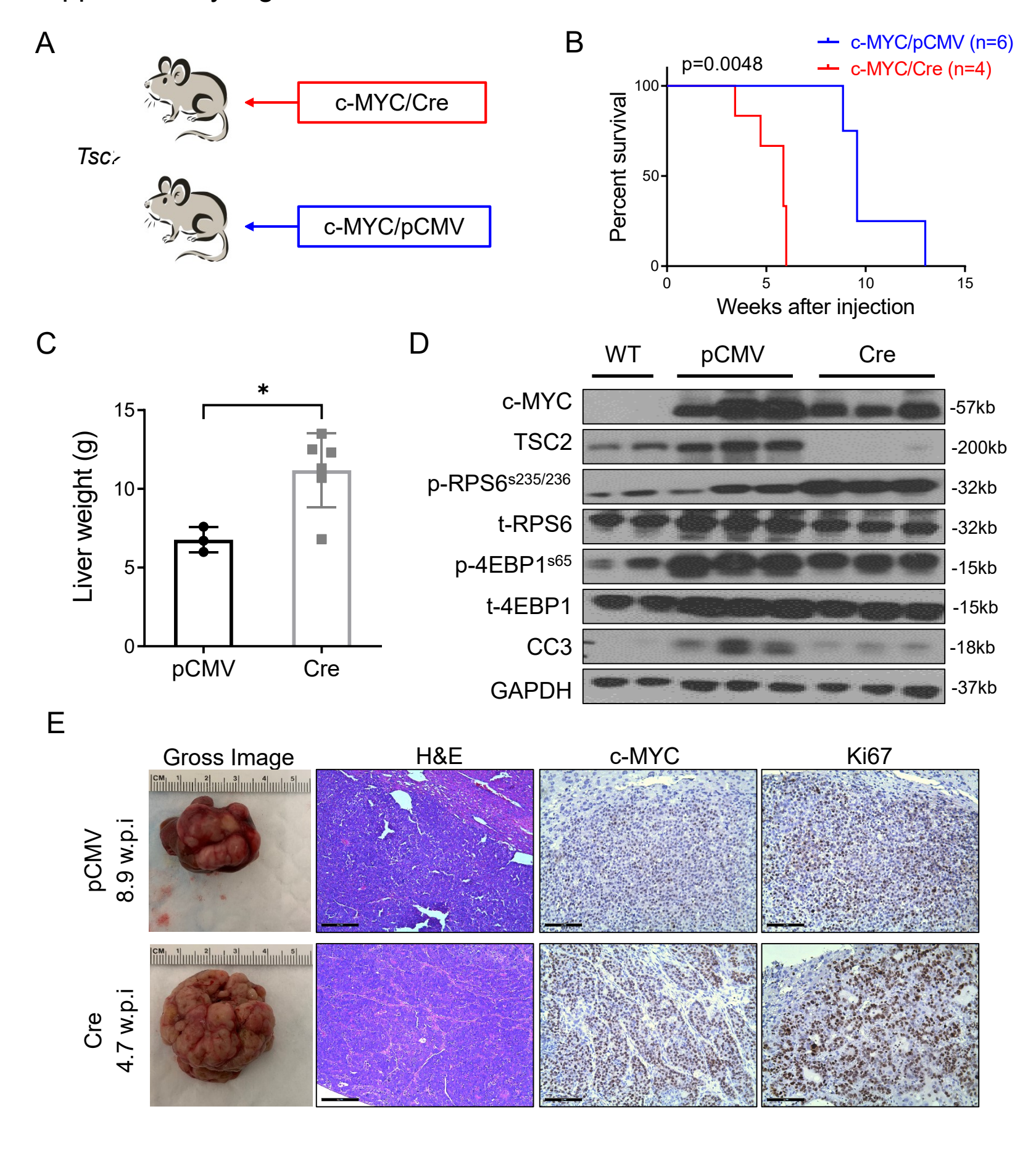
Enrichment

Enrichment

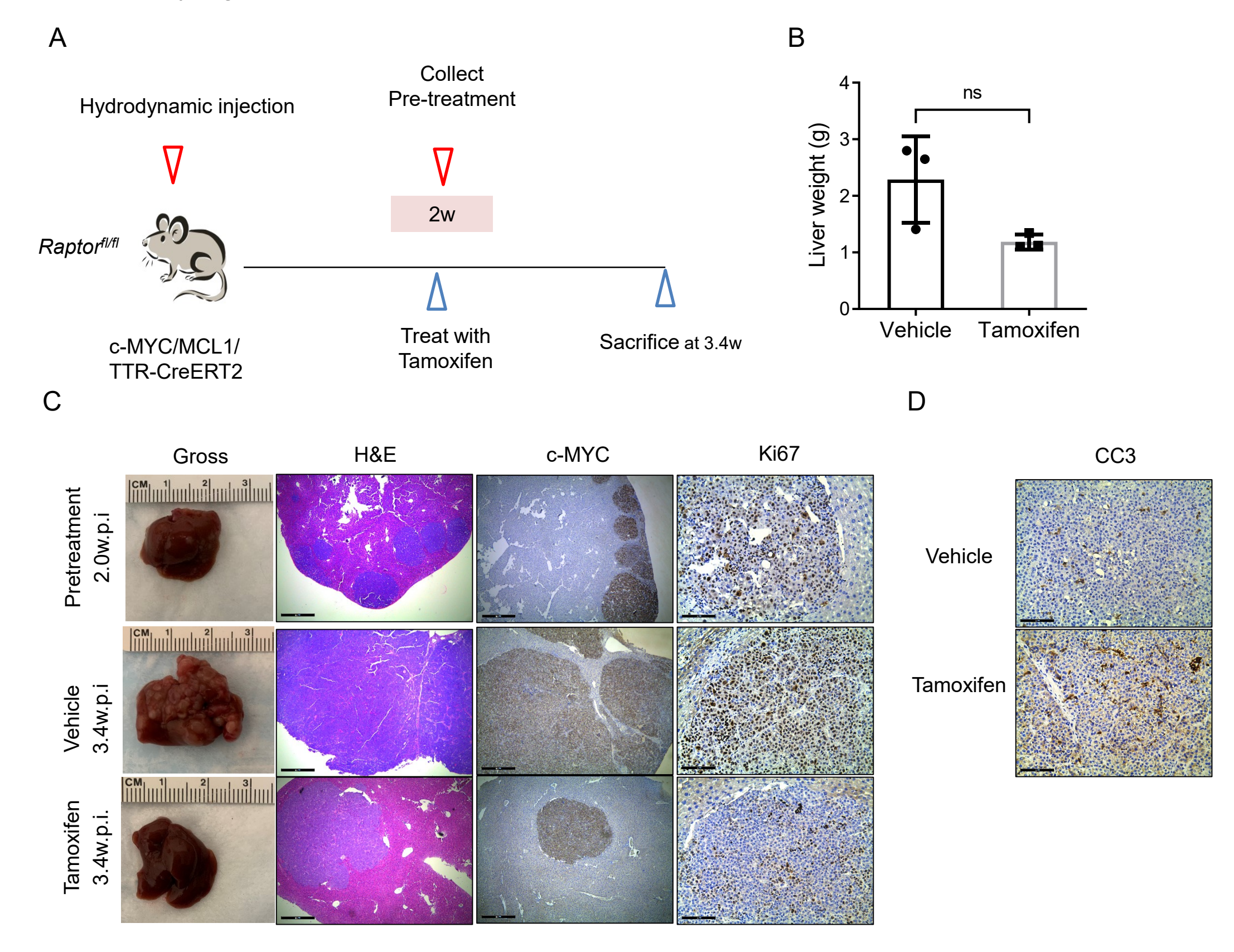
Supplementary Fig. 5. Analysis of RNA-seq data for NL, c-MYC/pT3, and c-MYC/FoxO1AAA. (A) Venn diagram displaying the genes that are upregulated in c-MYC/pT3 but downregulated by FOXO1AAA. (B) Venn diagram displaying the genes downregulated in c-MYC/pT3 but upregulated by FOXO1AAA. (C) KEGG analysis of the genes upregulated in c-MYC/pT3 but downregulated by FOXO1AAA. (D) KEGG analysis of the genes downregulated in c-MYC/pT3 but upregulated by FOXO1AAA. Abbreviations: NL, normal liver. pT3, pT3-EF1a.



Supplementary Fig. 6. TSC mutations correlate with c-MYC activation status in human HCCs. (A) Heatmap displaying expression levels of c-MYC signature genes among the HCC samples from the TCGA-LIHC dataset. The samples were grouped into three categories based on their c-MYC activation status: high (MYC-high), low (MYC-low), and medium (MYC-med). (B) Comparison of the percentages of HCC samples with high c-MYC activation status between the TSC1/2 mutated HCCs and the TSC1/2 wild-type HCCs. Data were analyzed using Chi-square test. Abbreviations: WT, wild-type.

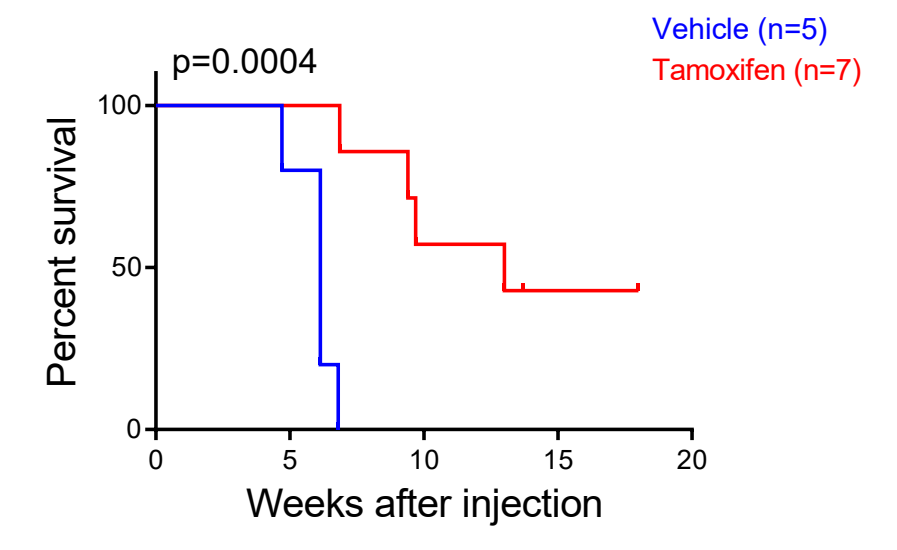


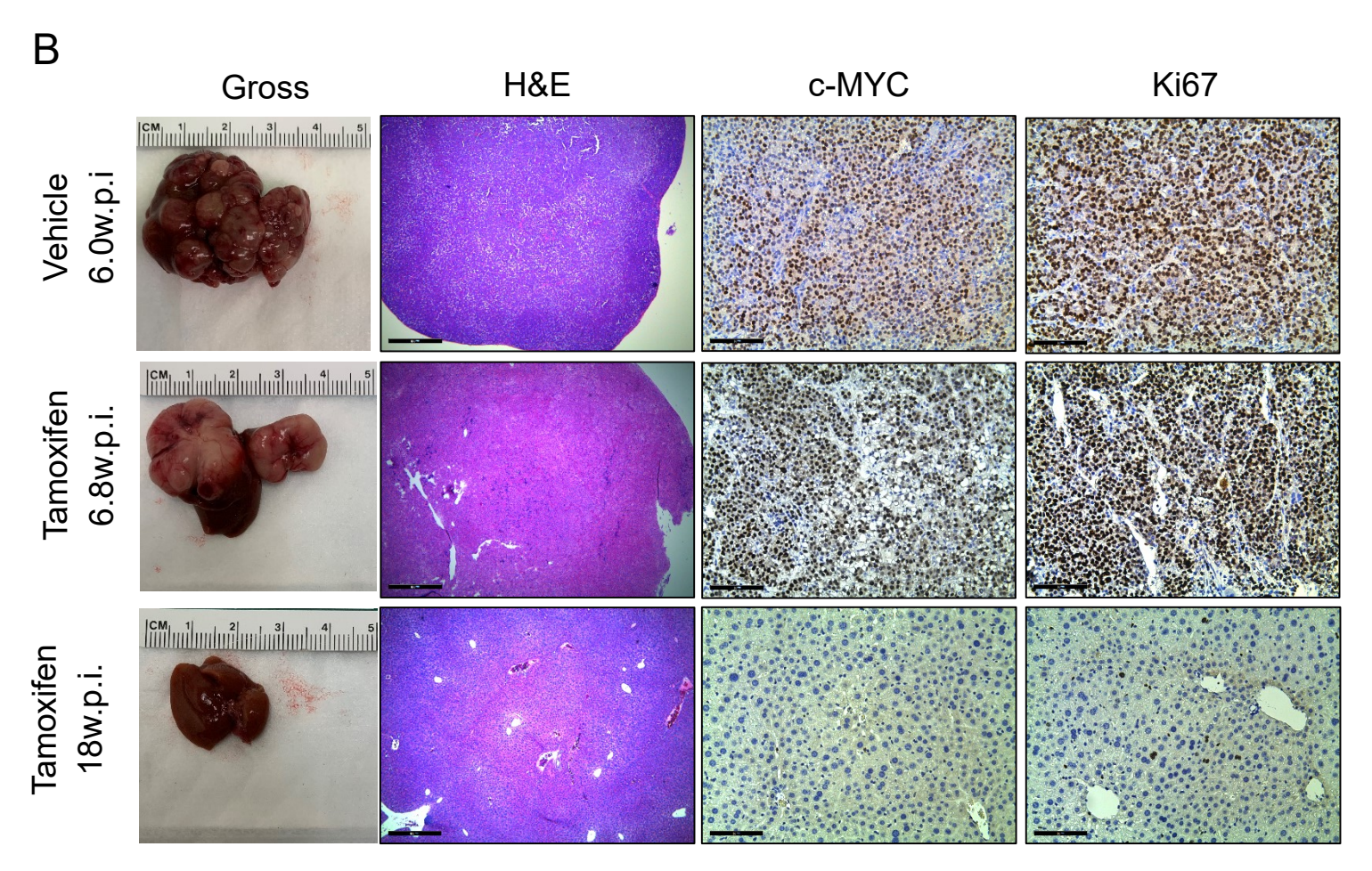
Supplementary Fig. 7. Deletion of *Tsc2* accelerates c-Myc-induced hepatocarcinogenesis. (A) Study design. $TSC2^{fl/fl}$ conditional knockout mice in FVB/N genetic background were hydrodynamically injected with plasmid mixtures of c-MYC and Cre recombinase in the pCMV backbone (c-MYC/Cre, n = 4). Control mice were hydrodynamically injected with c-MYC and pCMV empty vector (c-MYC/pCMV, n = 6). Mice were monitored for tumor development and euthanized either upon the development of large tumors or at the end of the observation period. (B) Survival curve of mice in both groups. The Kaplan-Meier comparison was performed, p = 0.0006. (C) Comparison of liver weight between the two groups. Data are presented as mean \pm SD. Student's t-test. *, p < 0.05. (D) Western blot results showing expressions of c-MYC, TSC2, cleaved caspase 3 (CC3), and key molecules in the p70S6K/RPS6 and 4EBP1/eIF4E cascades. GAPDH was used as the loading control. (E) Representative images: gross views of the liver, H&E staining, and immunohistochemical stainings of c-MYC and Ki67. Scale bars: 500µm for H&E, 100µm for c-MYC and Ki67.



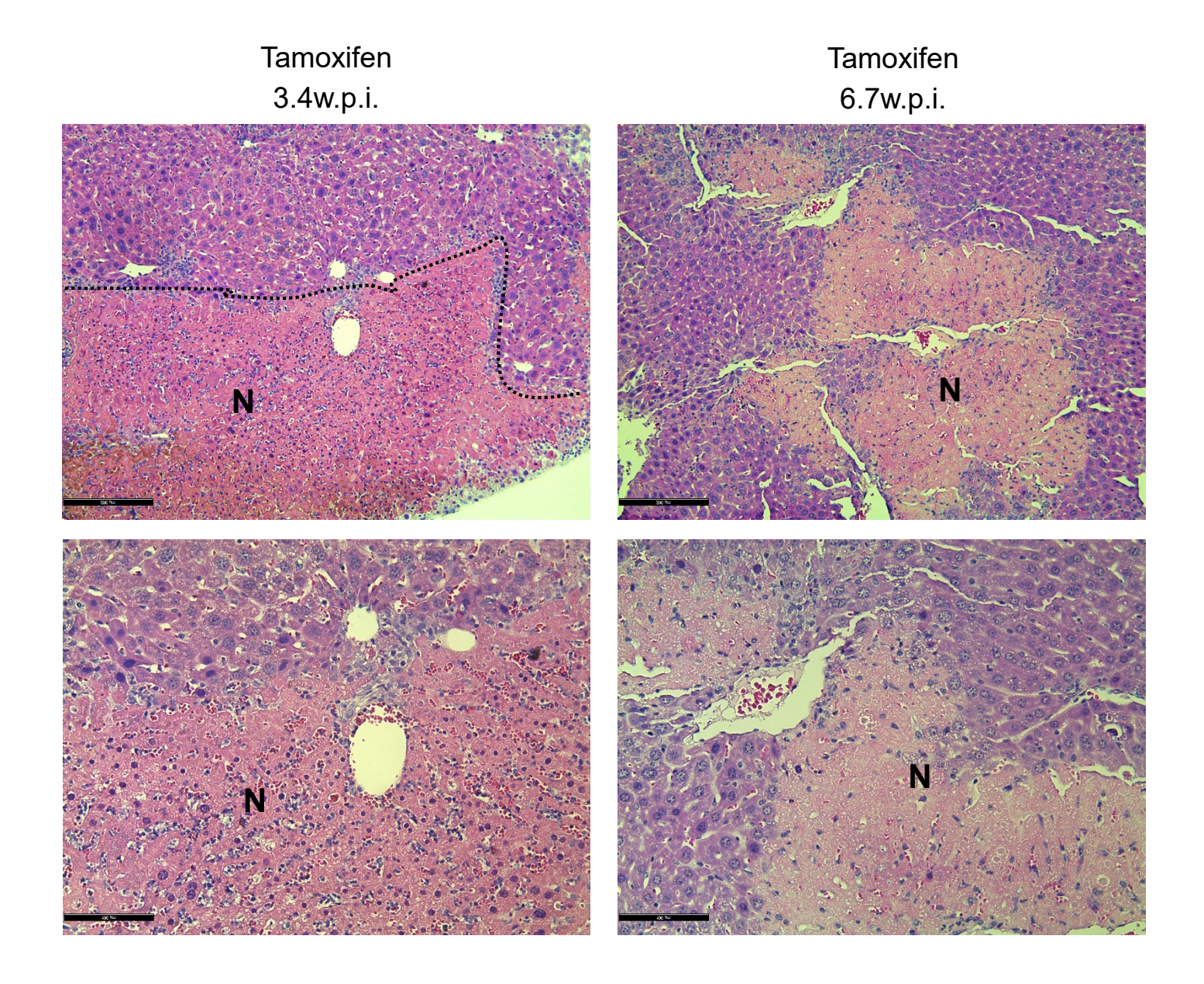
Supplementary Fig. 8. mTOCR1 impairment induces regression of c-MYC HCC. Tamoxifen-treated mice displayed tumor regression upon dissection, leading to a significantly lower liver weight, reduced proliferation, and increased apoptosis. (A) Study design. $Raptor^{fl/fl}$ conditional knockout mice were hydrodynamically injected with plasmid mixtures of c-MYC/MCL1 and tamoxifen-inducible CreERT2 recombinase under the liver-specific TTR promoter (c-Myc/MCL1/TTR-CreERT2). Two weeks post-injection (when tumor nodules were observed), one group of mice was sacrificed, and liver analysis was performed as the pre-treatment group. The remaining mice were treated with tamoxifen or vehicle for 1.4 weeks, followed by analysis after sacrifice. (B) Comparison of liver weight between the two groups (n = 3, 3). Data are presented as mean \pm SD. Student's t-test. ns, no significant.(C) Representative images: gross views of the liver, H&E staining, and immunohistochemical staining of Ki67 and c-MYC. (D) Representative images of cleaved caspase 3 (CC3) staining in vehicle- and tamoxifen- treated mice. Scale bars: 500µm for H&E and c-MYC, 100µm for Ki67 and CC3.



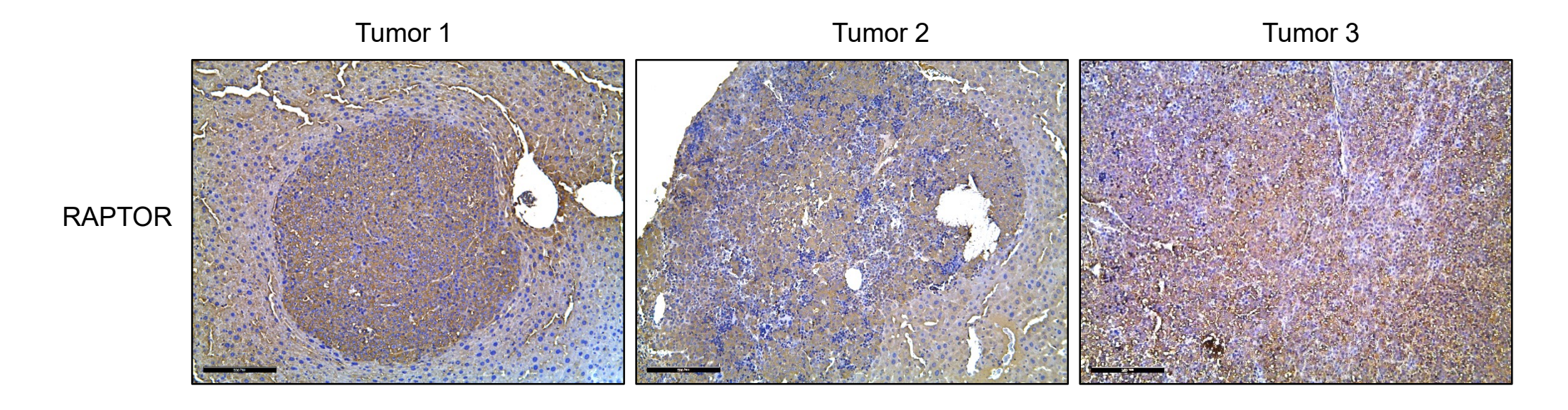




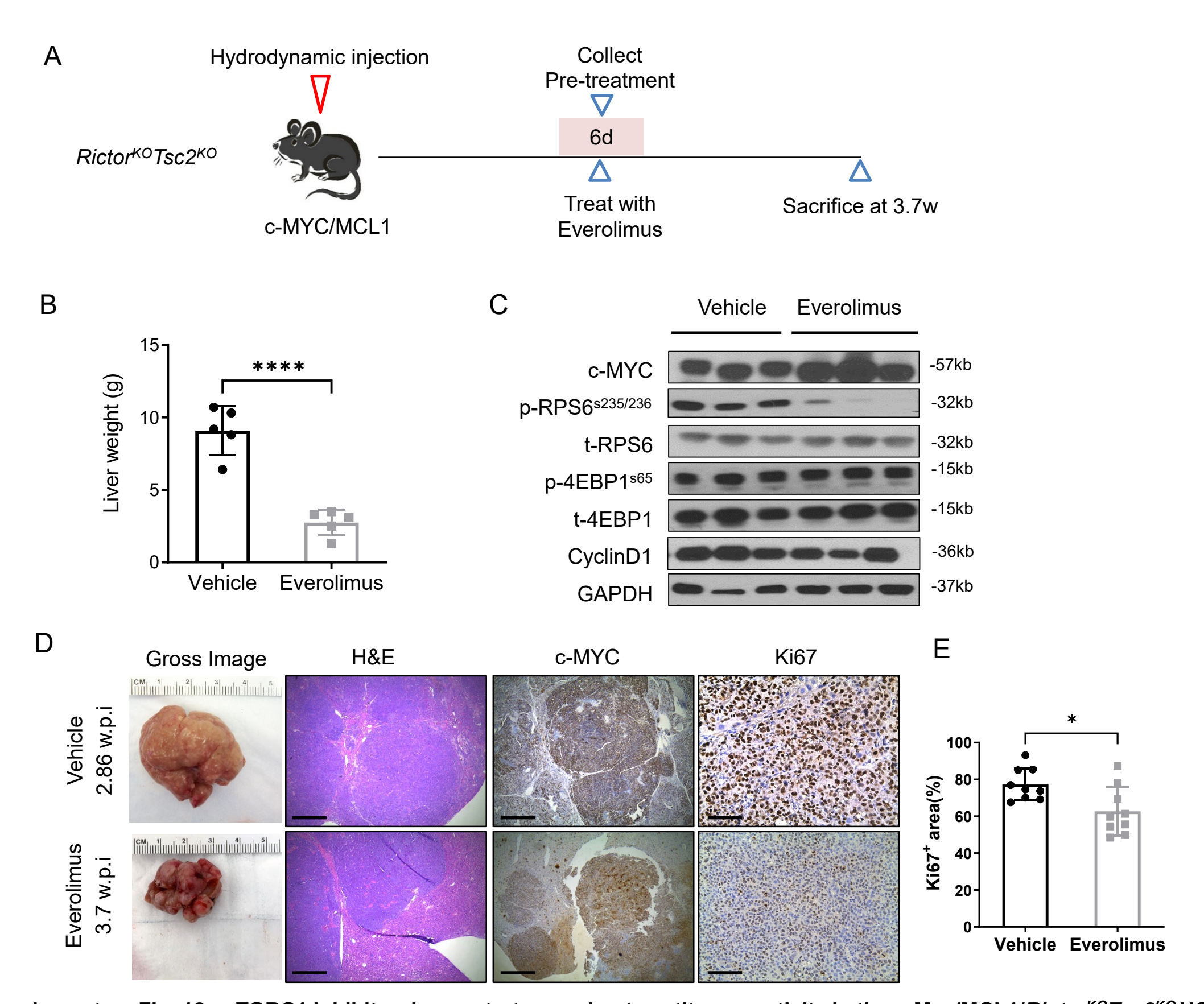
Supplementary Fig. 9. mTOCR1 impairment improves overall survival of c-MYC mice. (A) Survival curve of mice in both groups (n = 5, 7). The Kaplan-Meier comparison was performed, p = 0.0004. (B) Six of seven tamoxifen-treated mice developed a few, separate tumor nodules (ranging from 1 to 3) between 6.8 and 13.7 weeks post-injection. One mouse liver collected at 18 weeks appeared completely normal, whereas vehicle-treated mice exhibited a high tumor burden with numerous nodules between 4.7 and 8.9 weeks post-injection. Representative images: gross views of the liver, H&E staining, and immunohistochemical staining of c-MYC and Ki67. Scale bars: 500 μ m for H&E, 100 μ m for c-MYC, and Ki67.



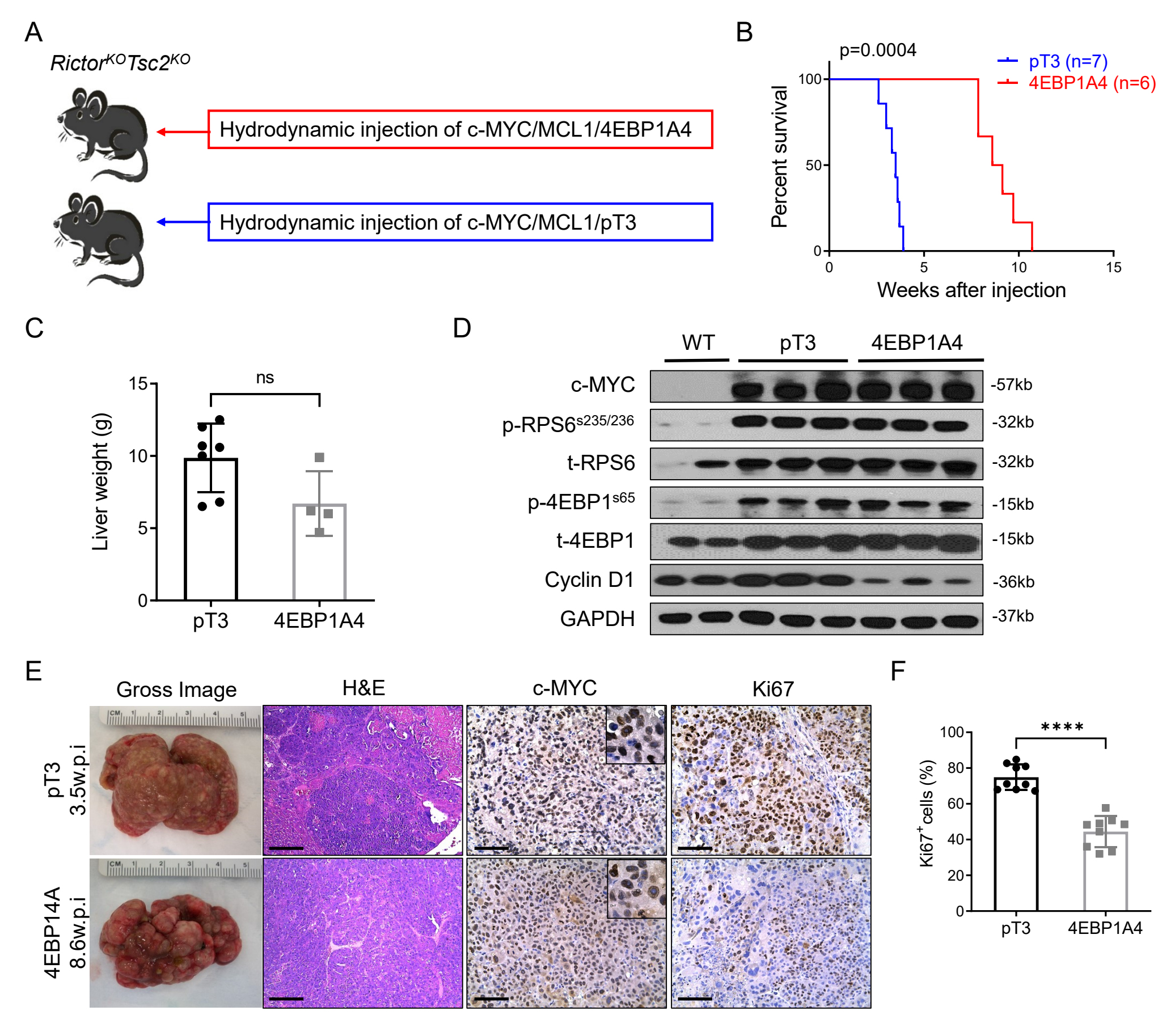
Supplementary Fig. 10. Representative images of H&E staining of c-MYC HCCs at different time points after tamoxifen treatment showed increased necrotic areas (N). Scale bars: 200µm.



Supplementary Fig. 11. Raptor staining revealed failed Cre recombinase activity in the tumor area of the tamoxifen-treated group. Large areas of necrosis were frequently observed in tamoxifen-treated livers. Thus, we speculate that the observed failure of tumor regression was due to off-target effects of the tamoxifen-inducible Cre transgene system.

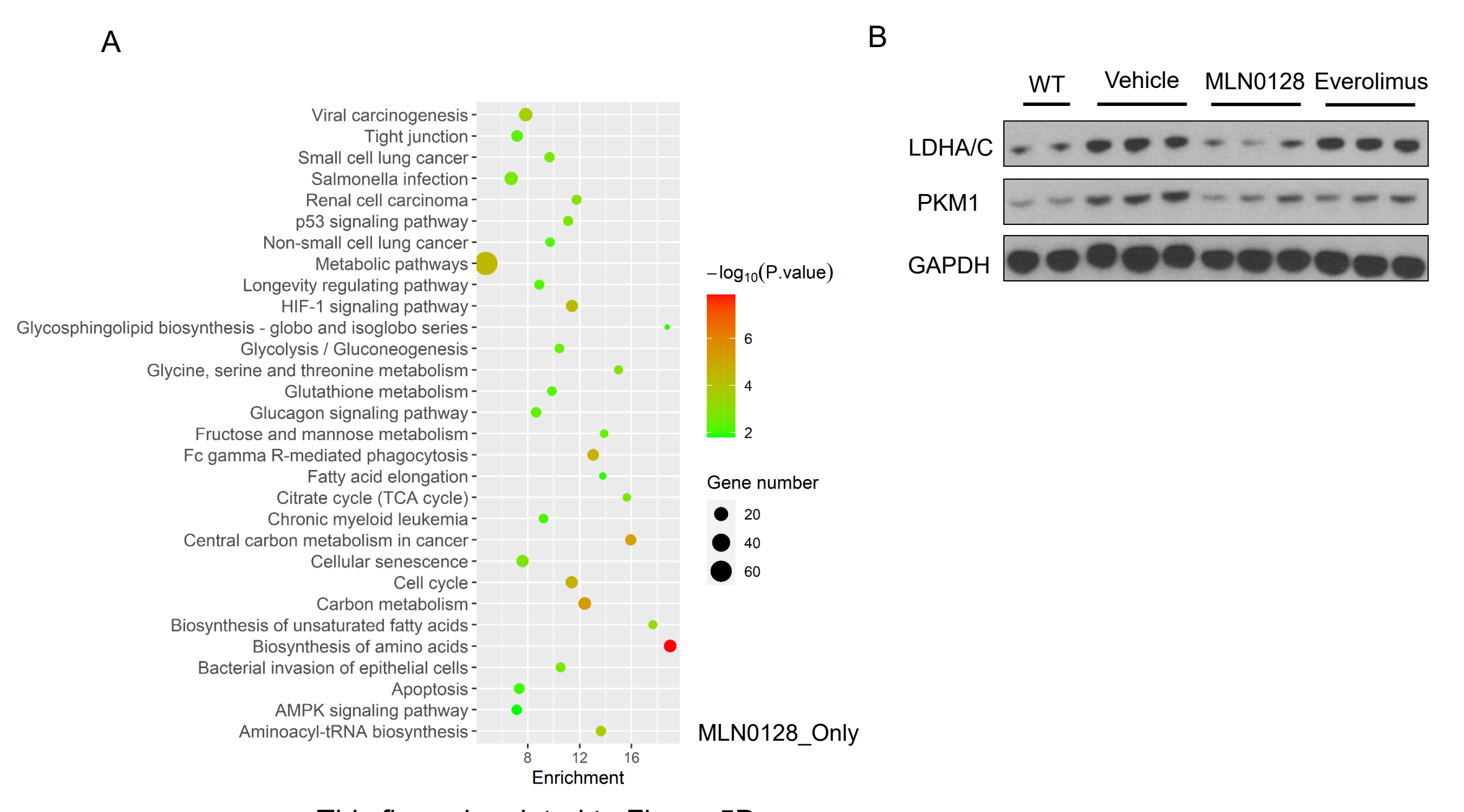


Supplementary Fig. 12. mTORC1 inhibitor demonstrates moderate antitumor activity in the c-Myc/MCL1/ $Rictor^{KO}Tsc2^{KO}$ MCCs. (A) Study design. c-MYC/MCL1/ $Rictor^{KO}Tsc2^{KO}$ murine tumor model was established through hydrodynamic injection. Six days post-injection, one group of mice (n = 3) was sacrificed, and liver analysis was performed as the pre-treatment group. The remaining mice were treated with the mTORC1 inhibitor everolimus (n = 5) or vehicle (n = 5) for 3 weeks, followed by analysis after sacrifice. (B) Comparison of liver weight between the everolimus and vehicle-treated groups. (C) Western blot results showing expressions of c-MYC, Cyclin D1, and key molecules in the p70S6K/RPS6 and 4EBP1/eIF4E cascades. GAPDH was used as the loading control. (D) Representative images: gross views of the liver (This figure shared a control group with MLN0128 in Figure 4E). H&E staining, and immunohistochemical staining of c-MYC and Ki67. Scale bars: 500µm for H&E and c-MYC, 100µm for Ki67. (E) Quantification results of the percentage of Ki67-positive cells in the two groups. Data are presented as mean \pm SD. Student's t-test. *, p<0.05. ****, p<0.0001.



Supplementary Fig. 13. Inhibition of 4EBP1/eIF4E delays tumorigenesis of c-Myc/MCL1/*Rictor*^{KO}*Tsc2*^{KO} HCCs.

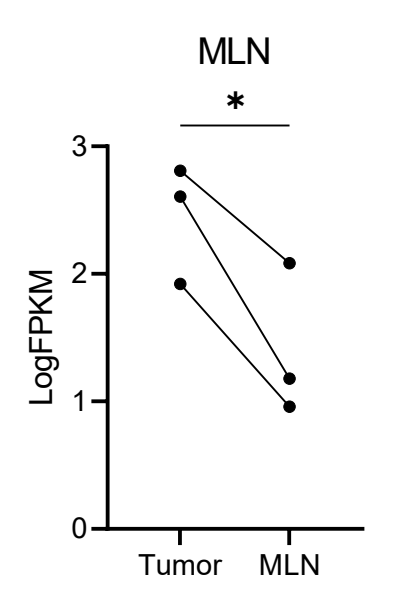
(A) Study design. $Rictor^{fl/fl}Tsc2^{fl/fl}$ mice were hydrodynamically injected with c-MYC/MCL1/Cre and the unphosphorylatable form of 4EBP1 (c-MYC/MCL1/4EBP1A4/ $Ricto^{KO}Tsc2^{KO}$, n = 7). Control mice were injected with c-MYC/MCL1/Cre and pT3 empty vector (c-MYC/MCL1/pT3/ $Ricto^{KO}Tsc2^{KO}$, n = 6). (B) Survival curve of mice in both groups. The Kaplan-Meier comparison was performed, p = 0.0006. (C) Comparison of liver weight between the two groups. (D) Western blot results show the levels of c-MYC, cyclin D1, and key molecules in the p70S6K/RPS6 and 4EBP1/eIF4E cascades. GAPDH was used as the loading control. (E) Representative images: gross views of the liver, H&E staining, and immunohistochemical staining of c-MYC and Ki67. Scale bars: 500µm for H&E, 100µm for c-MYC, and Ki67. (F) Quantification results of percentage of Ki67 positive cells in the two groups. Data are presented as mean \pm SD. Student's t-test. ns, no significant. ****, p<0.0001.

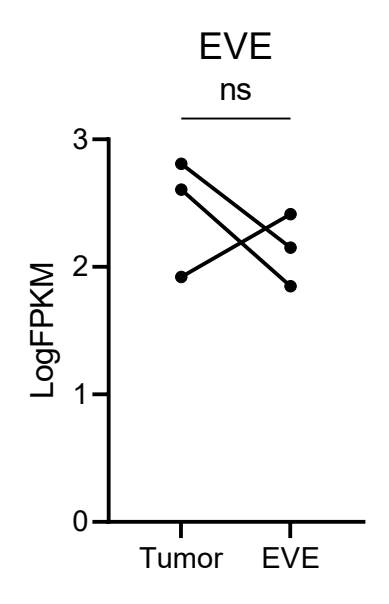


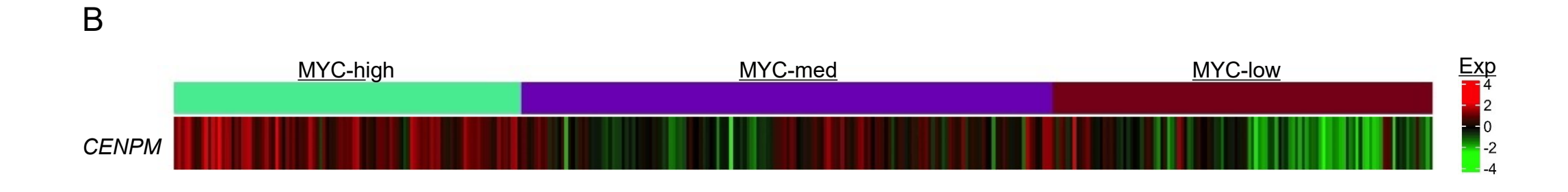
This figure is related to Figure 5D

Supplementary Fig. 14. Analysis of p70S6K/RPS6 and 4EBP1/eIF4E downstream target genes. (A) KEGG analysis of the differentially expressed genes downregulated by MLN0128, but not by everolimus. **(B)** Western blot results showing levels of LDHA/C and PKM2 in wild-type livers (WT), Vehicle-treated, MLN0128-treated, or Everolimus-treated c-MYC/MCL1/*Rictor*^{KO}*Tsc2*^{KO} HCCs. GAPDH was used as the loading control.

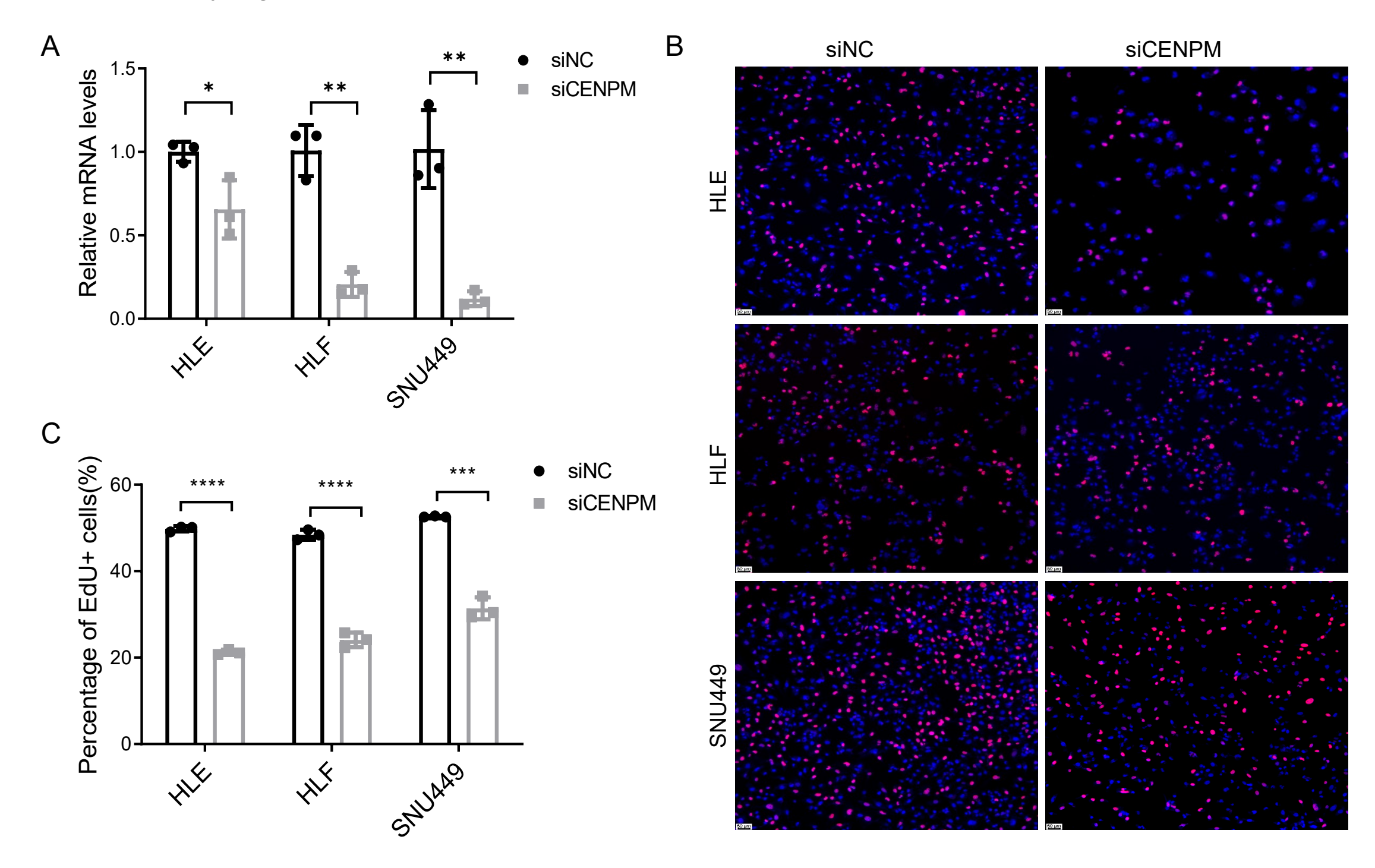
A



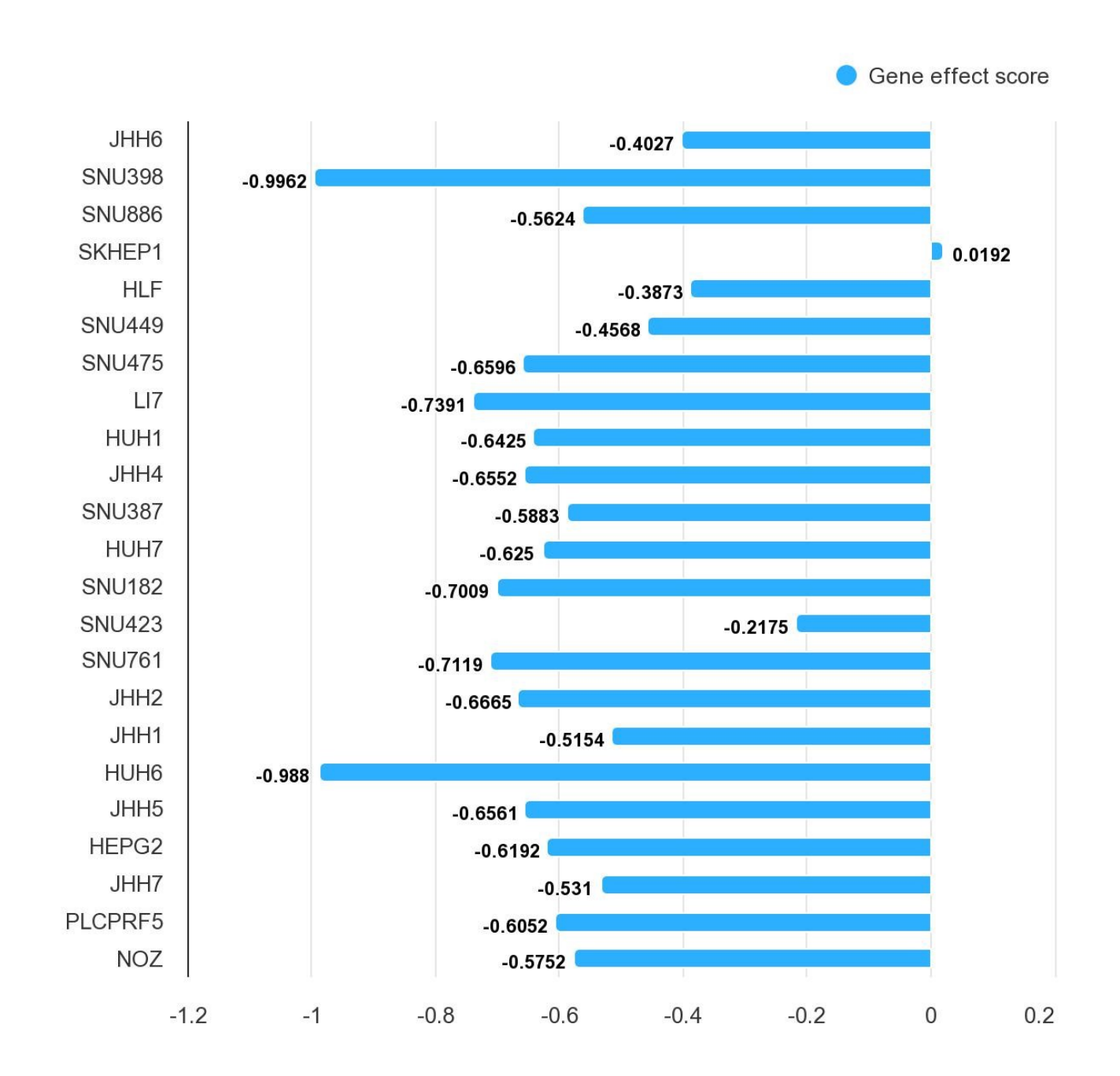




Supplementary Fig. 15. Analysis of the correlation between CENPM expression and MYC activation. (A) The CENPM expression in mouse c-MYC HCC upon MLN0128 (MLN) or Everolimus (EVE) treatment (n = 3, 3). Data are presented as mean \pm SD. paired t test. ns, no significant. *, p<0.05. (B) The correlation between CENPM expression and the MYC activation levels based on the TCGA-LIHC database.

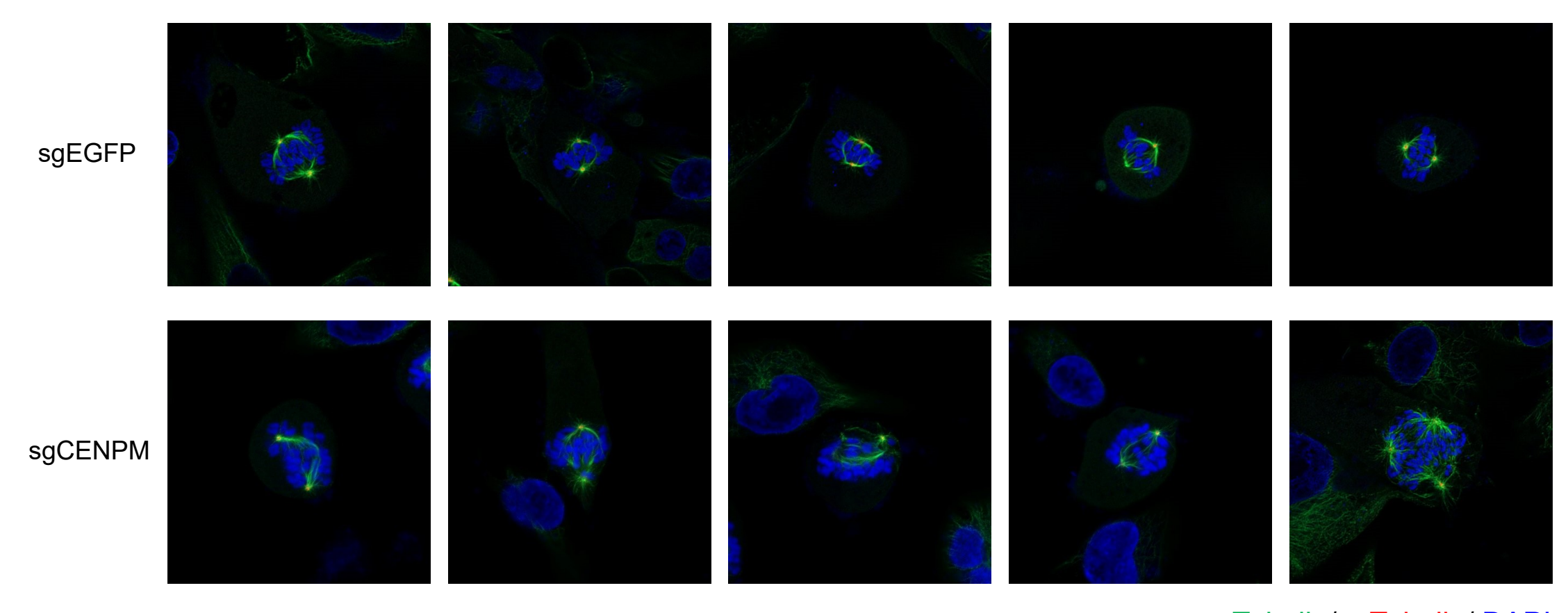


Supplementary Fig. 16. Silencing of CENPM inhibits human HCC cell proliferation. (A) qPCR results showing CENPM mRNA expression in siCENPM and control siRNA (siNC) transfected human HCC cells. (B, C) Representative images (B) and quantification (C) of EdU staining in the siNC, or siCENPM transfected human HCC cells. Data are presented as mean \pm SD. Student's t-test. *, p<0.05, **, p<0.01, ***, p<0.001, ****, p<0.0001.



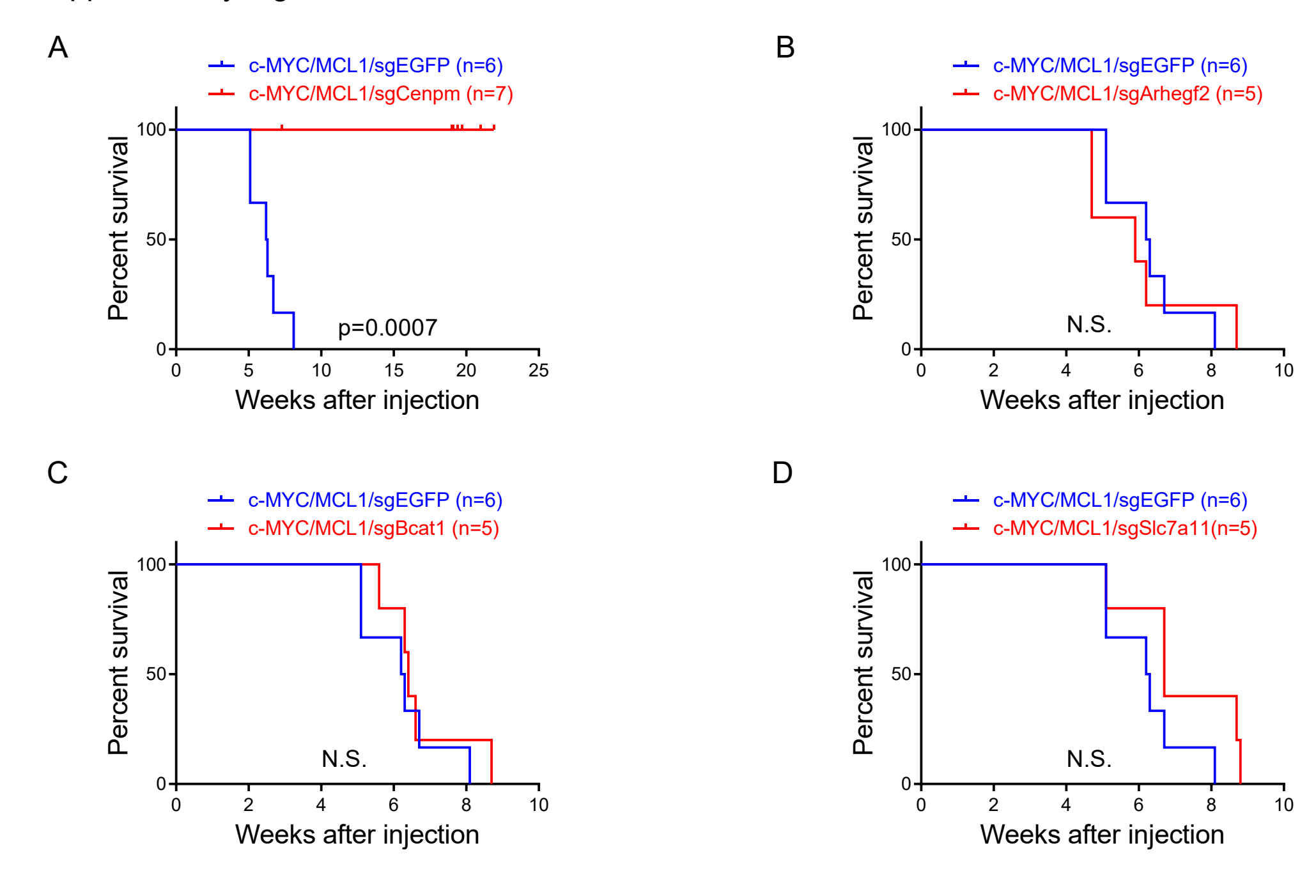
Supplementary Fig. 17. CENPM is critical for HCC cell growth. Depmap results show the dependency of CENPM in a panel of HCC cell lines. Gene Effect scores derived from CRISPR knockout screens published by Broad's Achilles and Sanger's SCORE projects. Negative scores imply cell growth inhibition and/or death following gene knockout. Scores are normalized such that nonessential genes have a median score of 0 and independently identified common essentials have a median score of -1. (Website: https://ualcan.path.uab.edu/cgi-bin/ualcan).

CENPM KO cells.

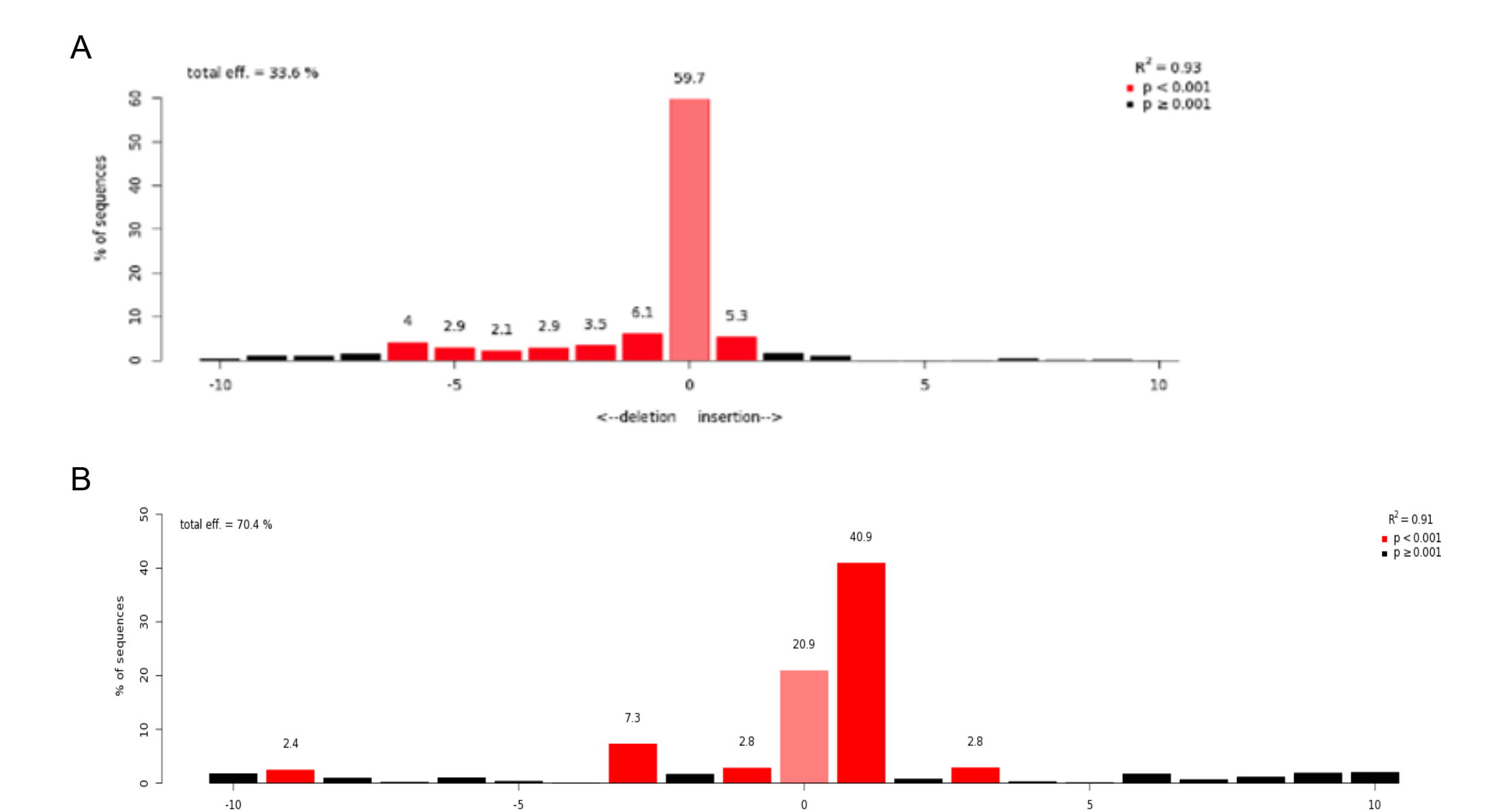


α-Tubulin/ γ-Tubulin/ DAPI

Supplementary Fig. 18. The immunofluorescence-based microscopy analysis of CENPM KO cells. Representative images of immunofluorescence staining of α -tubulin (indicating microtubule, kinetochore or spindle fibers), γ -tubulin (centrosome) and DAPI (indicating chromosomes) in the CENPM KO cells and the control cells during mitosis. Lagging chromosomes or mis-segregation were observed in almost all the

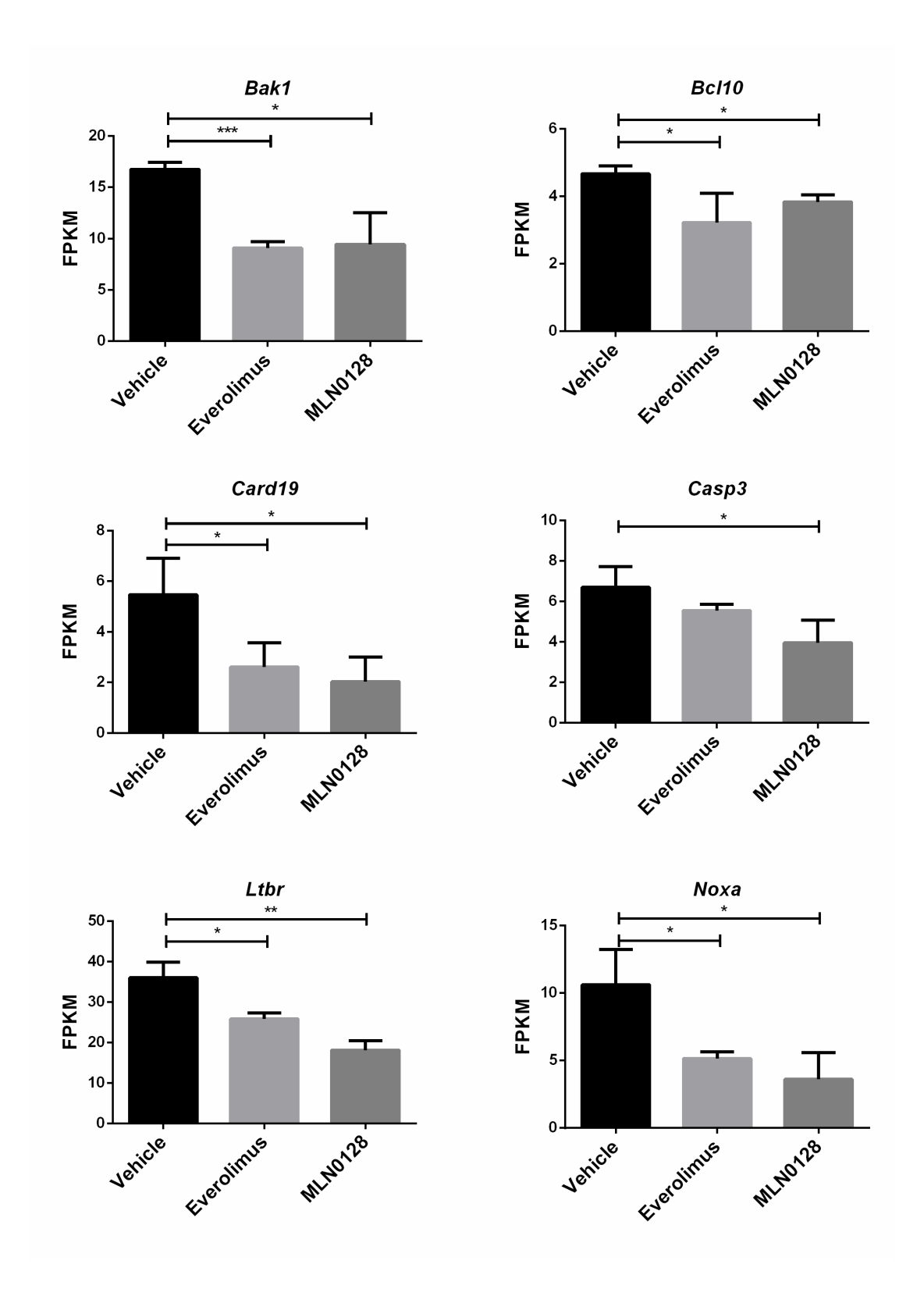


Supplementary Fig. 19. CENPM is a critical target of c-MYC-induced hepatocarcinogenesis. (A-D) Survival curves of mice in the c-MYC/MCL1 HCCs with deletion of *Cenpm* (A), *Arhegf*2 (B), *Bcat1* (C), and *Slc7a11* (D). The Kaplan-Meier analysis was performed, and *p*-values are indicated in the graphs.

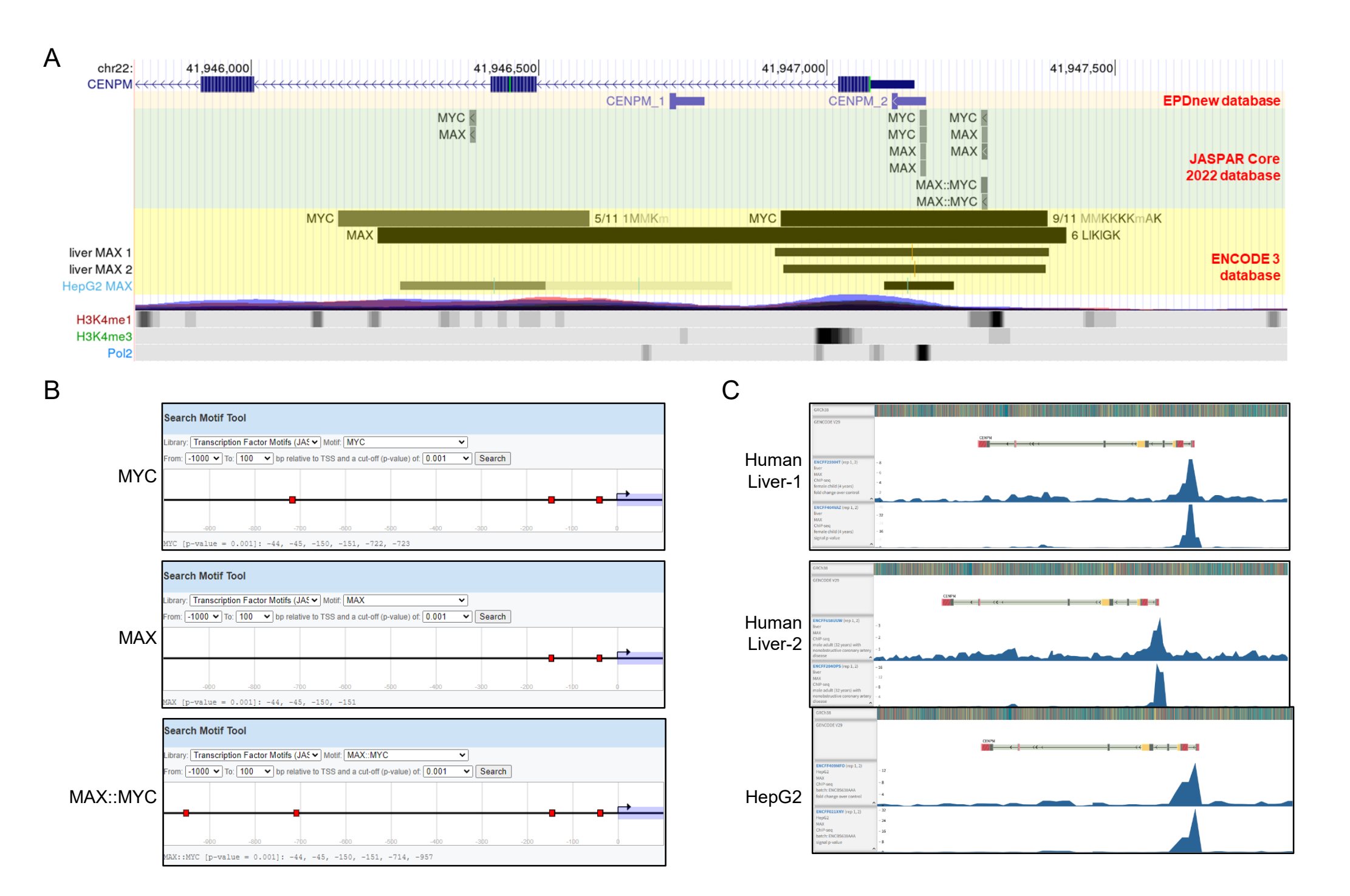


Supplementary Fig. 20. Confirmation of CRISPR-mediated *Cenpm* editing efficiency in the mouse c-MYC HCC cell line (HCC3-4) (A) and the c-MYC mouse model (B) by direct Sanger sequencing.

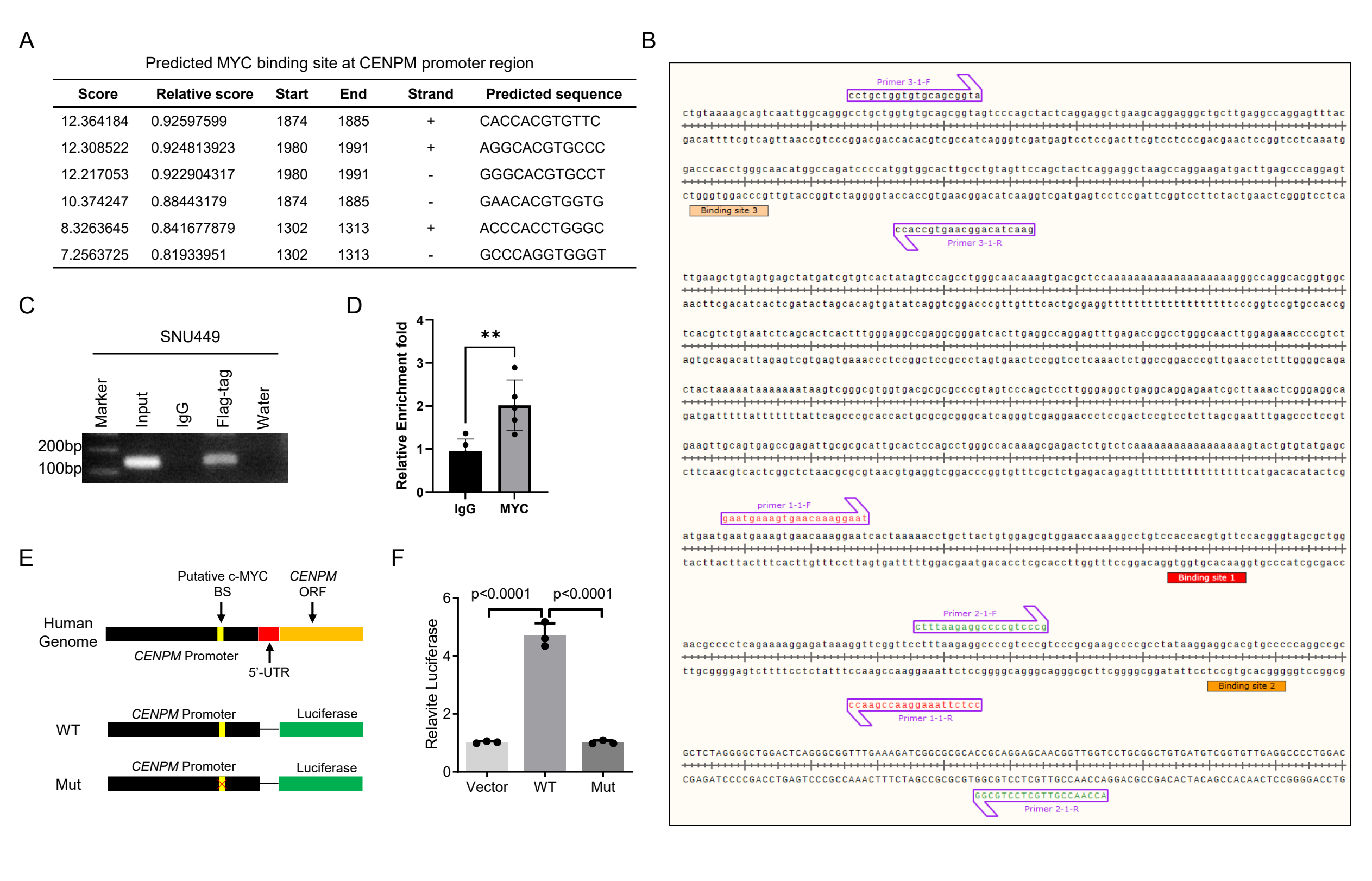
<--deletion insertion-->



Supplementary Fig. 21. Effects of mTOR inhibitors on apoptosis-related genes in c-MYC/MCL1/ $Rictor^{KO}Tsc2^{KO}$ HCCs. Comparison of the FPKM values for apoptotic genes among vehicle-treated, MLN0128-treated, and Everolimus-treated mouse c-MYC/MCL1/ $Rictor^{KO}Tsc2^{KO}$ HCCs (n = 3, 3, 3). Data are presented as mean \pm SD. Tukey–Kramer test. *, p<0.05, **, p<0.01, ***, p<0.001.



Supplementary Fig. 22. Promoter analysis of CENPM gene. (A) Integration analysis of MYC and MYC::MAX transcription factors with experimentally validated CENPM promoters was performed using various publicly accessible databases. Multiple conserved MYC and MYC::MAX binding sites were identified using the EPDnew database (https://epd.expasy.org/epd/EPDnew_database.php) and the JASPAR core 2022 database (https://jaspar2022.genereg.net/).ChIP-seq data on human liver and HepG2 liver cancer cells from the ENCODE3 database (https://www.encodeproject.org/) also indicated MYC and MAX binding sites on the CENPM promoter region. These sites showed abundant methylation or trimethylation of histone H3 at lysine 4 (H3K4me1 or H3K4me3) and RNA polymerase II (Pol2), which are active marks associated with transcriptional activation. (B) Representative images show the binding sites of MYC, MAX, and the MYC::MAX complex at -1000bp to +100bp relative to the CENPM transcriptional start site, with a cut-off p-value of 0.001. Images were generated from the EPDnew database. (C) Representative images show the bigWig peaks of ChIP-seq analysis for MAX transcription factor using liver tissue from a 4-year-old female child, 32-year-old male adult, and HepG2 cells with CRISPR targeting MYC.



Supplementary Fig. 23. CENPM is a direct transcriptional target of c-MYC. (A) Predicted MYC binding sites at CENPM promoter region. (B) Primer design for CHIP and CUT & RUN assay on the CENPM promoter region. (C) ChIP assay on the promoter of CENPM. pCMV4a-Flag-c-Myc transfected SNU449 cells were used. (D) CUT & RUN assay for CENPM promoter in SNU449 cells. Data are presented as mean \pm SD. Student's t-test. ns, no significant. **, p<0.01. (E) Experimental design of the luciferase reporter assay. (F) Luciferase reporter assay for the identification of MYC binding sites in the CENPM gene promoter region (n = 3, 3, 3). Data are presented as mean \pm SD. Tukey–Kramer test and p-values are indicated in the graphs.

TSC/mTORC1 mediates mTORC2/AKT1 signaling in c-MYC-induced murine hepatocarcinogenesis via centromere protein M

Yi Zhou^{1, 2*}, Shu Zhang^{3,4*}, Guoteng Qiu^{5,6}, Xue Wang⁷, Andrew Yonemura⁷, Hongwei Xu^{2,5}, Guofei Cui^{2,7}, Shanshan Deng^{2,7}, Joanne Chun⁷, Nianyong Chen^{3,4,8}, Meng Xu⁹, Xinhua Song¹⁰, Jingwen Wang¹⁰, Zijing Xu¹⁰, Youping Deng^{7,11}, Matthias Evert¹², Diego F. Calvisi¹², Shumei Lin¹, Haichuan Wang^{5,6} and Xin Chen^{2,7}

Supplementary Tables

Supplementary Table 1. LogFPKM data for NL, c-MYC/pT3, and c-MYC/FoxO1AAA mouse models. List of genes that are upregulated in c-MYC/pT3 but downregulated by FOXO1AAA, and list of genes that are downregulated in c-MYC/pT3 but upregulated by FOXO1AAA. Please refer to the excel file for the detailed information.

Supplementary Table 2. List of guide RNA used for CRISPR-Cas9 mediated gene deletion

Guide RNA	Sequence
Human CENPM	AACACGATCAGGTCAATTCG
Mouse Cenpm	AACACAATCAGGTCAATTCG
Mouse Arhgef2	CCACAGACTCCCTCAACATG
Mouse Bcat1	TGGTGTGATGATGAGATCTT
Mouse Slc7a11	GCACAACTGGCTTTCTGACC

Directory	Mice breed	Plasmid injected (µg)	Sample size (n)
Figure 1	Rictor ^{fl/fl} ;Foxo1 ^{fl/fl}	c-MYC(10)+MCL1(10)+Cre(20)+SB(1.6)	6
		c-MYC(10)+MCL1(10)+pCMV(20)+SB(1.6)	6
Figure 2	FVB/N	c-MYC(10)+Foxo1AAA(40)+SB(2)	5
		c-MYC(10)+ pT3(40)+SB(2)	5
Figure 3	Rictor ^{fl/fl} ;Tsc2 ^{fl/fl}	c-MYC(10)+MCL1(10)+Cre(20)+SB(1.6)	6
		c-MYC(10)+MCL1(10)+pCMV(20)+SB(1.6)	4
Figure 4	Rictor ^{fl/fl} ;Tsc2 ^{fl/fl}	c-MYC(10)+MCL1(10)+Cre(20)+SB(1.6) treated with MLN0128	3
		c-MYC(10)+MCL1(10)+Cre(20)+SB(1.6) treated with vehicle	5
Figure 7	FVB/N	c-MYC(10)+MCL1(10)+SB(0.8)+sgCENPM(40)	7
		c-MYC(10)+MCL1(10)+SB(0.8)+sgEGFP(40)	6
Sup Fig.3	FVB/N	c-MYC(10)+Foxo3AAA(40)+SB(2)	3
		c-MYC(10)+ pT3(40)+SB(2)	3
Sup Fig.7	Tsc2 ^{fl/fl}	c-MYC(10)+Cre(20)+SB(1.2)	4
		c-MYC(10)+pCMV(20)+SB(1.2)	6
Sup Fig.4	Raptor ^{fl/fl}	c-MYC(10)+MCL1(10)+TTR-CreERT2(20)+SB(1.6) treated with Tamoxifen	7
		c-MYC(10)+MCL1(10)+TTR-CreERT2(20)+SB(1.6) treated with vehicle	5
		c-MYC(10)+MCL1(10)+TTR-CreERT2(20)+SB(1.6) pretreatment	3
Sup Fig.7	Rictor ^{fl/fl} ;Tsc2 ^{fl/fl}	c-MYC(10)+MCL1(10)+Cre(20)+SB(1.6) treated with Everolimus	5
		c-MYC(10)+MCL1(10)+Cre(20)+SB(1.6) treated with vehicle	5
Sup Fig.8	Rictor ^{fl/fl} ;Tsc2 ^{fl/fl}	c-MYC(10)+MCL1(10)+Cre(20)+SB(3.2)+4EBP1A4(40)	7
		c-MYC(10)+MCL1(10)+Cre(20)+SB(3.2)+pT3(40)	6

Sup Fig.12	FVB/N	c-MYC(10)+MCL1(10)+SB(0.8)+sgEGFP(40)	6
		c-MYC(10)+MCL1(10)+SB(0.8)+sgArhegf2(40)	5
		c-MYC(10)+MCL1(10)+SB(0.8)+sgBcat1(40)	5
		c-MYC(10)+MCL1(10)+SB(0.8)+sgSLC7a11(40)	5

Supplementary Table 4. List of antibodies used for immunohistochemistry

	Catalog			
Antibody	Number	Company	Species	Dilution
c-MYC	ab32072	Abcam	Rabbit	1:200
Myc-tag	Vli01	MMCRI	Rabbit	1:200
Ki-67	12202	Cell Signaling Technology	Rabbit	1:150
Cleaved Caspase-3	9664	Cell Signaling Technology	Rabbit	1:150
Raptor	MA5-35742	Thermo Fisher Scientific	Rabbit	1:100
FOXO1	2880	Cell Signaling Technology	Rabbit	1:100
FOXO3	12829	Cell Signaling Technology	Rabbit	1:100
phospho-FOXO1 (Ser				
256)	PA5-104977	Thermo Fisher Scientific	Rabbit	1:100
phospho-FOXO3 (Ser				
253)	PA5-118528	Thermo Fisher Scientific	Rabbit	1:100

Supplementary Table 5. List of antibodies used for Western blot analysis

Antibody	Catalog Number	Company	Species	Dilution
AKT	9272	Cell Signaling Technology	Rabbit	1:1000
Phospho-AKT (Ser473)	4060	Cell Signaling Technology	Rabbit	1:1000
Rictor	9476	Cell Signaling Technology	Rabbit	1:1000
FOXO1	2880	Cell Signaling Technology	Rabbit	1:1000
Phospho-FOXO1 (Ser256)	84192	Cell Signaling Technology	Rabbit	1:1000
S6 Ribosomal Protein	2217	Cell Signaling Technology	Rabbit	1:1000
Phospho-S6 Ribosomal Protein (Ser235/236)	4858	Cell Signaling Technology	Rabbit	1:1000
4E-BP1	9644	Cell Signaling Technology	Rabbit	1:1000
Phospho-4E-BP1 (Ser65)	9451	Cell Signaling Technology	Rabbit	1:1000
c-MYC	ab32072	Abcam	Rabbit	1:2000
Cleaved Caspase-3	9664	Cell Signaling Technology	Rabbit	1:1000
Cyclin D1	2978	Cell Signaling Technology	Rabbit	1:1000
LDHA/C	3558	Cell Signaling Technology	Rabbit	1:1000
PKM1	7067	Cell Signaling Technology	Rabbit	1:1000
CENPM	ab243820	Abcam	Rabbit	1:1000
GAPDH	5174	Cell Signaling Technology	Rabbit	1:10000

β-actin 4970 Cell Signaling Technology Rabbit 1:1000

Supplementary Table 6. List of primers used in qRT-PCR analysis

Gene name	Forward	Reverse
18s rRNA	CGGCTACCACATCCAAGGAA	GCTGGAATTACCGCGGCT
Human-CENPM	GCGGACTCGATGCTCAAAGA	TTCTGGAGACTGTATTTGCTGTG